SPE Automotive Composites Conference 9/12-9/13, Troy, MI

Electrochemical and stack evaluation of composite bipolar plate materials

Joachim Scherer*, Raimund Stroebel*, and Eve Steigerwalt#

*** Dana Corporation[1] (Victor Reinz Division), Neu-Ulm, Germany.**
 # Dana Corporation (Plumley Sealing Division), Paris, TN.

Abstract: Composite plate materials for use as bipolar plates in a fuel cell stack must meet certain performance criteria, namely, high surface and through-plane electrical conductivity, very low gas permeability, and chemical resistance to both coolants and reactants. In addition to these performance criteria, it is necessary from a cost viewpoint that the bipolar plates are easy to manufacture. One category of materials being used for bipolar plates are carbon composites, where carbon additives are mixed with a thermoset resin for net-shape compression molding of bipolar plates. A study of the corrosion resistance (via electrochemical testing), helium permeation, stack performance, and electrical conductivity of a variety of composite materials designed for bipolar plate applications will be presented.

Background

Bipolar plates have a number of functions in the fuel cell stack. They must be electrically conductive, gas impermeable, and corrosion-resistant. Designing a material that will satisfy all three performance criteria is a challenge. Designing a material that will satisfy all three performance criteria while simultaneously being low-cost and easy-to-manufacture is much larger challenge.

However, certain materials have acceptable fuel cell performance, namely, graphite and metal alloys. Both materials have advantages and disadvantages. Graphite is time-consuming and expensive to machine into the complex design of the bipolar plate, yet it is resistant to a wide variety of substances. Metal is easy to stamp with the bipolar plate design, yet is susceptible to corrosion problems that could easily poison the fuel cell membrane.

Improvements have been made to both: graphite composite materials exist that can be net-shape molded, thus improving the manufacturability, and new coatings for metals exist which reduces or eliminates the corrosion problems.

---

[1] Dana Corporation is one of the world's largest suppliers of components, modules, and complete systems to global vehicle manufacturers and their related aftermarkets. Dana Corporation was founded in 1904, and based in Toledo, Ohio. Dana's Internet address is www.dana.com.

This study concentrates on the fuel cell performance of net-shape molded graphite composite materials. These composites are a mixture of graphite, thermoset resin, and other additives. The resin acts as a binder that holds the graphite in the complex design of the bipolar plate. Two types of resin are commonly used at the moment: a vinyl-ester material and a phenolic material. In this study, the materials are primarily vinyl-ester materials, and one phenolic material was examined.

Two vinyl-ester based graphite composite materials were examined: materials **A** and **B**, and compared against a phenolic-based material, **C**. In the electrochemical corrosion experiments, **A** and **B** were compared to **C**, while in the stack testing, bipolar plates of **A** (Stack **A**) and bipolar plates of **B** (Stack **B**) were compared against bipolar plates made out of material **C** (Stack **C**). Helium permeation testing was completed on two later generations of material **A** (**A2** and **A3**, still vinyl-ester based), and compared to material **C**. Electrical conductivity measurements were performed on all five materials (**A-C**), including graphite.

Experimental Details

Electrochemical Corrosion Testing

The graphite composite plate samples were sanded with 1200 grit paper before measurement. The material samples consisted of disks 15 mm in diameter. The cyclic voltammetry measurements were taken with a platinum counter electrode and a $Hg/Hg(SO_4)$ reference electrode that had been calibrated against a Calomel reference (SCE) before each measurement. An electrolyte of 1M H_2SO_4, 20ppm HF (pH 0) with a constant nitrogen purge was used for all CV measurements. Oxygen was removed from the electrolyte by sparging with Ar for 1 h before the measurements. A sweep rate of 10 mV/s was used for CV measurements, with the exception of the study of cycle stability, where a 0.5 mV/s sweep rate was used. Data was taken at 25°C.

Stack Assembly

All the four-cell stacks were assembled in an identical fashion. The only difference between the stacks is the composite material of the bipolar plate. The membrane electrode assembly (MEA) was purchased from W.L. Gore & Associates, Inc. (PRIMEA MESGA series 5561, 35μm thick, with an anode loading of 0.45 mg/cm^2 Pt-Ru and a cathode loading of 0.3 mg/cm^2 Pt). The active area was 126 cm^2 (10 x 12.6 cm). The gas diffusion layer (GDL) was Toray paper (H-120 with a thickness of 0.37mm). The GDL was treated with Teflon (PTFE content approximately 25%) in house. Sealing frames consisted of sheet metal frames with printed elastomer seals (0.72 mm high, uncompressed), supplied by Victor Reinz, Dana Corporation. The cathode and anode plates are 3.2 mm thick.

The single cell repeating unit within the stack consisted of a cathode bipolar plate, GDL/sealing frame, MEA, GDL/sealing frame, anode bipolar plate, and sealing frame (which separates the anode bipolar plate from the cathode bipolar plate), shown in Figure

1. The GDL is incorporated into the metal sealing frame. The cathode plate has both coolant and air flowfields, while the anode plate only has a patterned reactant flowfield. The stack was compressed with four bolts, fixed with a torque of 14 Nm each. The assembled stack is shown in Figure 2.

Stack Testing

Once the stack was ready for testing, it was placed in a sealed plexiglass chamber in order to retain the appropriate humidity. The cathode of the MEA was fed by an external manifold, where the air is circulated within the glass chamber by a fan. Fresh air, provided to the system, was regulated using massflow controllers. Once the air entered the stack chamber it was immediately mixed with the exhaust air from the stack, thus humidifying it. This insured that the air being forced through the cathodes would always be humidified. The hydrogen was pre-humidified before entering the internal H_2 manifold of the stack. The stack operated at ambient pressure at 55°C, except for the stack of material **C** (Stack **C**), where the operating temperature was kept below 50°C. The stack was cooled with water.

Several stack parameters were measured during the test. Humidity, temperature, stack potential, stack current, chamber temperature, coolant temperature, and individual cell voltages were collected. Impedances were measured using a remote-control AC-ohmmeter (Schuetz MR2212W; frequency = 500 Hz). Potentials were measured using a digital multimeter.

The potentials were measured before and after the cathode and anode plates as well as before and after the MEA. With these data, the GDL potential drop and area resistance can be calculated or measured. The area resistance was measured using both the impedance method (R x Area) and the multimeter voltage measurements (ΔV/current density).

The turnover percentage for the anode was kept at 90%, while the cathode was held at 25%. These values were determined by prior experiments using this stack configuration. The stack is operated at 60A (J = 0.476 A/cm^2), except when it was to be unattended for long periods of time, when it was run potentiostatically.

The stack is initially taken through a conditioning period on start up. As the stacks are assembled with dry MEAs, it takes several hours to reach maximum, stable performance. The start-up time of the stacks is required in order to humidify the membranes completely and to remove impurities form the MEA that remain from its manufacture.

Helium Permeation

A round sample of material (5 cm in diameter) was clamped into a round holder, sealed at the outer rim of the sample. On one side of the sample 0.01, 0.1, and 0.2 MPa (absolute) of pure helium was pressurized onto the sample. On the other side, the sample

was directly attached to the vacuum of a mass spectrometer that was recording the permeating helium.

Electrical Conductivity

Electrical conductivity measurements were performed using a Valhalla Scientific 4300B micro-ohmmeter connected to gold-plated electrodes. Toray paper 0.17mm thick was used for each material.

Results and Discussion

Two vinyl-ester based graphite composite materials were examined: materials **A** and **B**, and compared against a phenolic-based material, **C**. In the electrochemical corrosion experiments, **A** and **B** were compared to **C**, while in the stack testing, bipolar plates of **A** (Stack **A**) and bipolar plates of **B** (Stack **B**) were compared against bipolar plates made out of material **C** (Stack **C**). Helium permeation testing was completed on two later generations of material **A** (**A2** and **A3**, still vinyl-ester based), and compared to material **C**. Electrical conductivity measurements were performed on all four materials (**A-C**), including graphite.

Electrochemical Corrosion Testing

Cyclic voltammograms of the as-manufactured bipolar plates of materials **A** and **B** are shown in Figure 3. As can be seen from the curves, the materials are nearly inert in the electrochemical environment. This is due to the enrichment of the plate surface with non-conductive resin during the compression-molded manufacturing process. The samples were then carefully sanded with 1200 grit sand paper to remove this enriched layer, and the measurements repeated. The new CV curve a shows much greater electrochemical response (see Figure 3). The control material **C**, showed no difference electrochemically between as-received and after sanding.

In Figure 4, CV curves of the materials after a 30 min immersion in 1 M H_2SO_4 are shown. The curves of material **B** and graphite consist primarily of double-layer capacitance, while the curve of material **A** shows a peak in the oxidation sweep that corresponds to an semi-irreversible process since there in no corresponding peak of the same magnitude in the reduction sweep. This semi-irreversible peak may be due to an unknown surface condition resulting from the sanding.

The stability of materials **A** and **B** in acid electrolyte was examined through a sequential series of CV curves, shown in Figure 5. Material **B** is stable over time, while material **A** and graphite seem to be affected in some manner, as can be seen from the decaying CV curves of the latter materials.

The long-term stability of materials **A** and **B** while held at potential was also examined. The material was taken to three potentials, 100 mV, 700 mV, and 950 mV, all values vs. RHE. As expected, the materials all show the same general behavior, that is,

all three materials were relatively inert under potential load in acidic solution. Material **A** shows some slight deviation from material **B** and **C**.

Stack Testing

Material **A** / Stack **A**

Figure 6 shows the polarization curves for a single cell in a four-cell stack made with material **A** bipolar plates (Stack **A**) at t = 0 h, 20 h, and 140 h. It can be seen that the cell performance improves over time. At the single cell potential of 0.6V, the current density increased from 0.243 A/cm^2 at t = 0, to 0.348 A/cm^2 at t = 20h, and ended at 0.393 A/cm^2 at t = 140 h. At higher current densities (measured at 0.5V), there was no degradation evident after the current density reached its maximum value at t = 20 h (0.515 A/cm^2).

Area resistances were measured via the impedance method at t = 20h (at which point the MEA had been conditioned), t = 70 h, and at t = 140 h, at three different stack loads (in the order in which they are listed): 70A (j = 0.56 A/cm^2), 60A (j=0.48 A/cm^2), and 80A (j = 0.64 A/cm^2). The results are shown in Figure 7.

It is immediately evident from Figure 7 that the major component of area resistance within the stack comes from the membrane. As the current density increases, the membrane resistance decreases, probably due to the greater hydration of the membrane from product water. The area resistances of both bipolar plates attain a steady value after 70h of operation. Results from measurements taken with the multimeter are similar (see Figure 8). However, measuring the area resistance of the membrane is not possible with the multimeter, therefore no data are shown.

Material **B** / Stack **B**

The polarization curves taken of the four-cell stack made with bipolar plates of material **B** (Stack **B**) are shown in Figure 9. They show a small decrease in performance over time. At 0.6V, the current density was 0.327 A/cm^2 at t = 0 h, decreased to 0.304 A/cm^2 at t = 50 h, and finally reached 0.288 A/cm^2 by t = 140 h.

The area resistances of the individual components were measured using both the impedance and multi-meter instruments (see Figure 10). The area resistance was measured at a stack load of 60A at t = 0 h, and at a load of 80A at t = 50 h. The multi-meter was used only to calculate the area resistances at t = 0 with a stack load of 60A. A comparison of the values calculated by the impedance method and the multimeter method at t = 0 h shows that the two methods give identical data within the region of error (with the exception of Cell 2 cathode plate). As expected, the membrane contributes the largest portion of the in-cell resistance.

Material **C** / Stack **C**

The polarization curves for the four-cell stack made with bipolar plates of the control material, material **C** (Stack **C**), are shown in Figure 11. The performance slightly decreased over the course of the experiment. At 0.6V, the current density was 0.257 A/cm^2 at t = 25 h, and then dropped to 0.245 A/cm^2 after a 100h test. Similarly, at 0.5V, the current density dropped by 0.014 V over the course of the experiment.

The area resistances were measured at t = 25 h and at t = 125 h, both measured at 60A load. The results are shown in Figure 12. Negative values appear due to a reversed polarity measurement. The area resistances are as expected, with the majority component coming from membrane resistance. It can also be seen that the area resistance decreases over time for most components. An interesting note is that the membrane resistance of the center two cells increased over time while the membranes of the outer cells decreased over time. This may due to a stack water-management issue.

Stack Comparison

Figure 13 shows the polarization curves from each stack at the end of the testing period. It can be seen that material **A** has superior performance to both material **B** and **C**, with material **C** performing the worst. However, the operating temperature of Stack **C** was 5ºC lower than that of the other two stacks; this may account for some of the difference.

Helium Permeation

Three materials were measured for helium permeation, material **A2** and **A3**, both vinyl-ester graphite composite materials, and material **D**, a phenolic-based graphite composite material. The permeation data is shown in Figure 14. Material **D** has the highest helium permeation of the three materials tested. Materials **A2** and **A3** are very similar, except that material **A3** has a lower permeation rate at higher pressures.

Electrical Conductivity

The through-plane electrical conductivity of samples, **A**, **B**, **C**, **A2**, and **A3** at 500 psia and 1000 psia are shown in Table 1.

Table 1. Electrical conductivity of samples A, B, C, A2, and A3.

Material	**Conductivity (S/cm)**	
	500 psia	**1000 psia**
A	24	25
B	33	42
C	5	6
A2	23	31
A3	26	37

As can be seen from the data in Table 1, the conductivity of the vinyl-ester based materials are all in the same range, with a gradual increasing of the conductivity level

with increase generation number (**A** < **A2** < **A3**). The phenolic-based material, **C**, has a very low conductivity. Material **B** has the highest conductivity.

Conclusion

From these experiments, it has been shown that material **A** has superior performance in the fuel cell environment, however, electrochemical corrosion testing shows some degradation of the material in the initial CV sweeps.

Material **B** has superior electrochemical corrosion protection and through-plane electrical conductivity as well as good performance in corrosion cycling testing, however, it does not perform as well as material **A** in the stack.

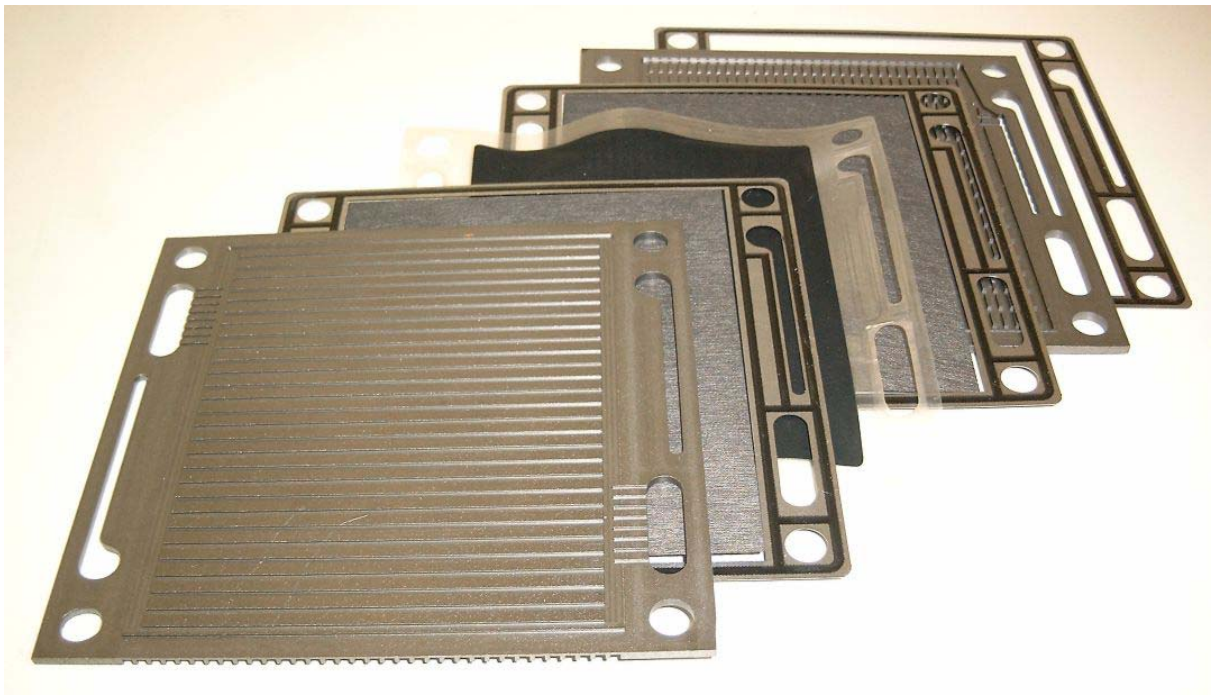

Figure 1. The components of a single-cell repeating unit (from top to bottom): cathode plate (coolant channels facing up), GDL/sealing frame, membrane, GDL/sealing frame, anode plate, coolant sealing frame.

Figure 2. The assembled four-cell stack with fan for forcing air.

(a)

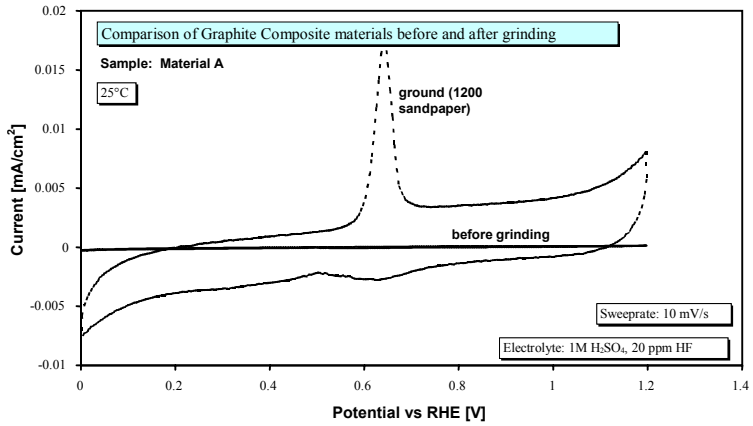

(b)

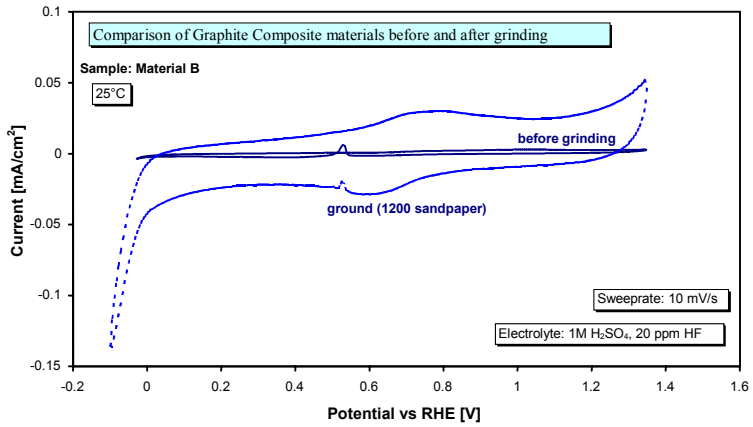

Figure 3. (a) CV curve of material **A** before and after grinding, (b) CV curve of material **B** before and after grinding.

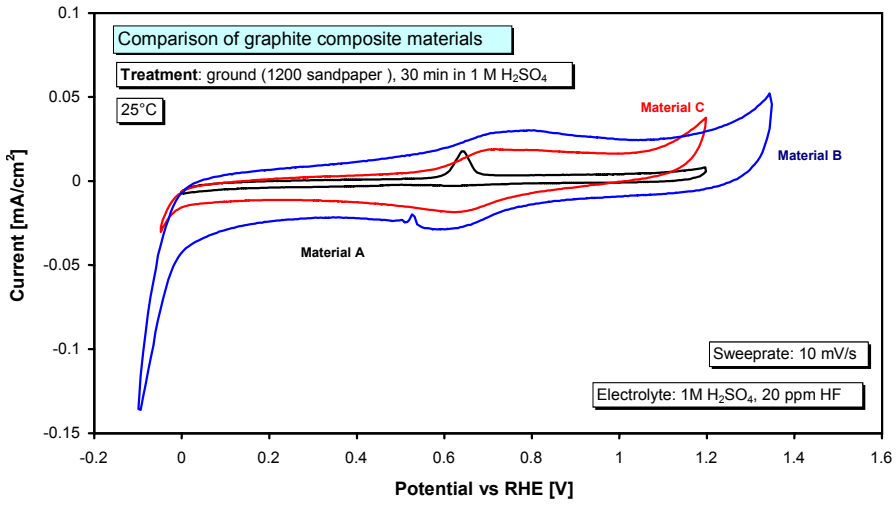

Figure 4. CV curves (2 cycles) of material **A**, **B**, and **C** after sanding.

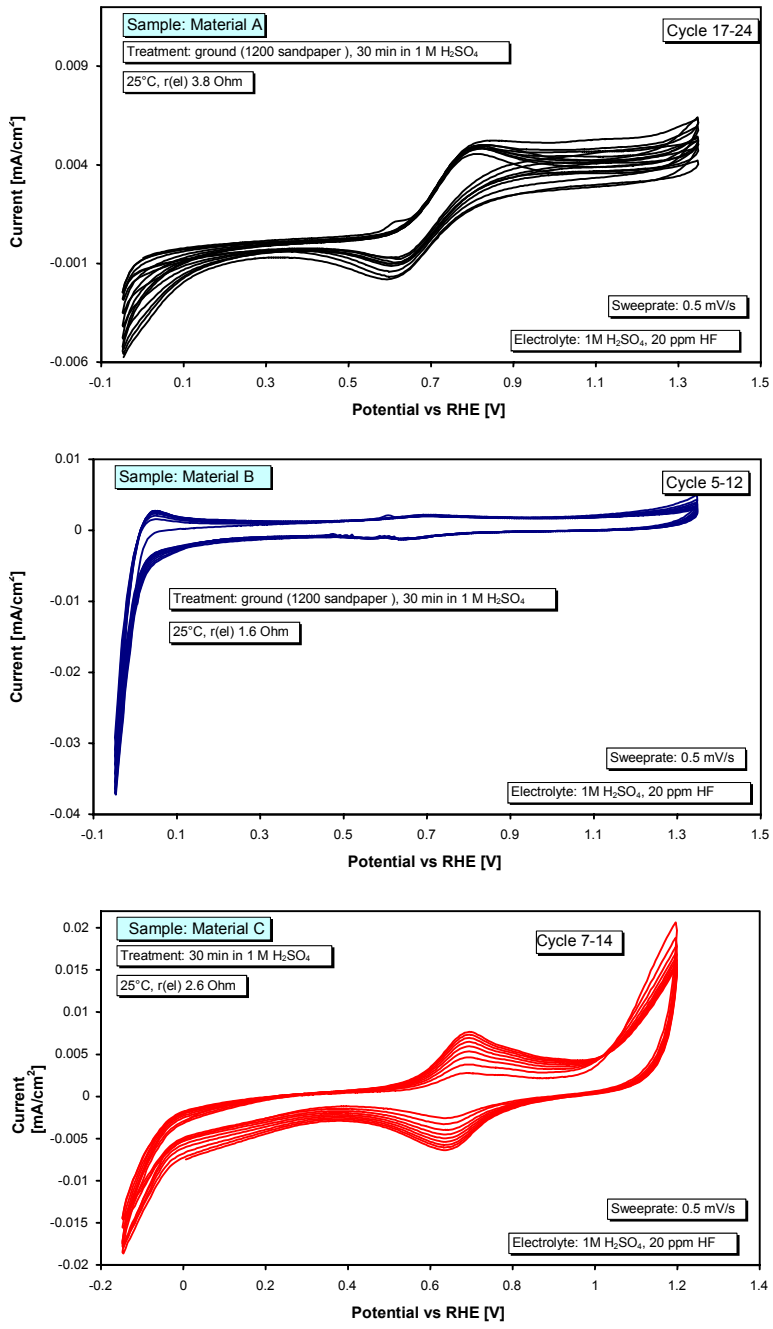

Figure 5. Cyclic stability of materials **A**, **B**, and **C**.

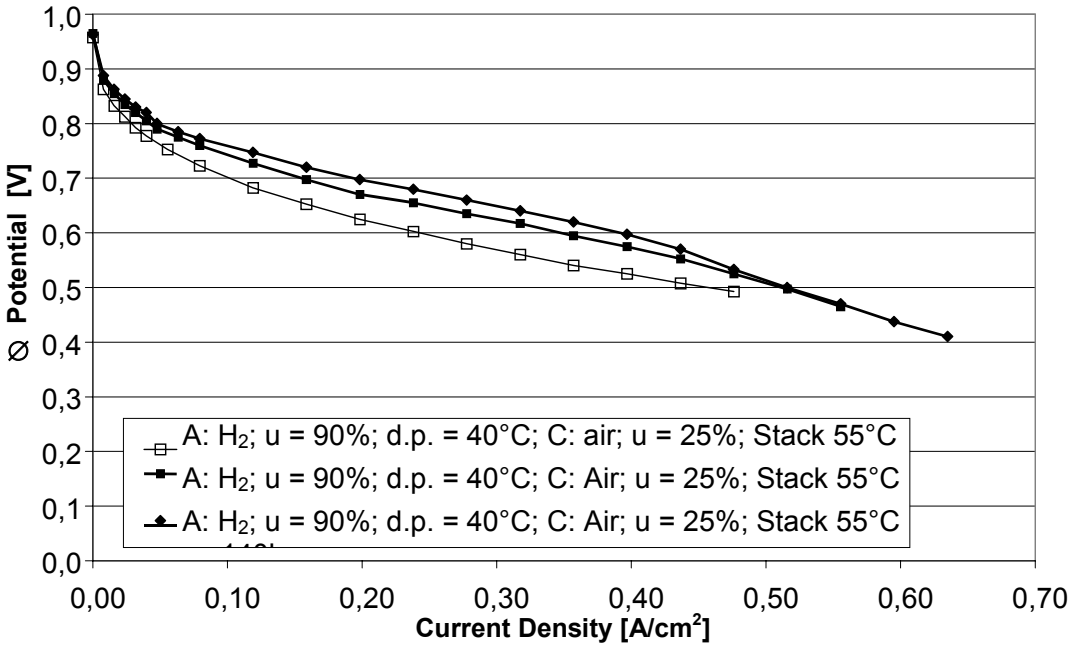

Figure 6. Polarization curves for Stack **A** at t = 0, 20, and 140 hours.

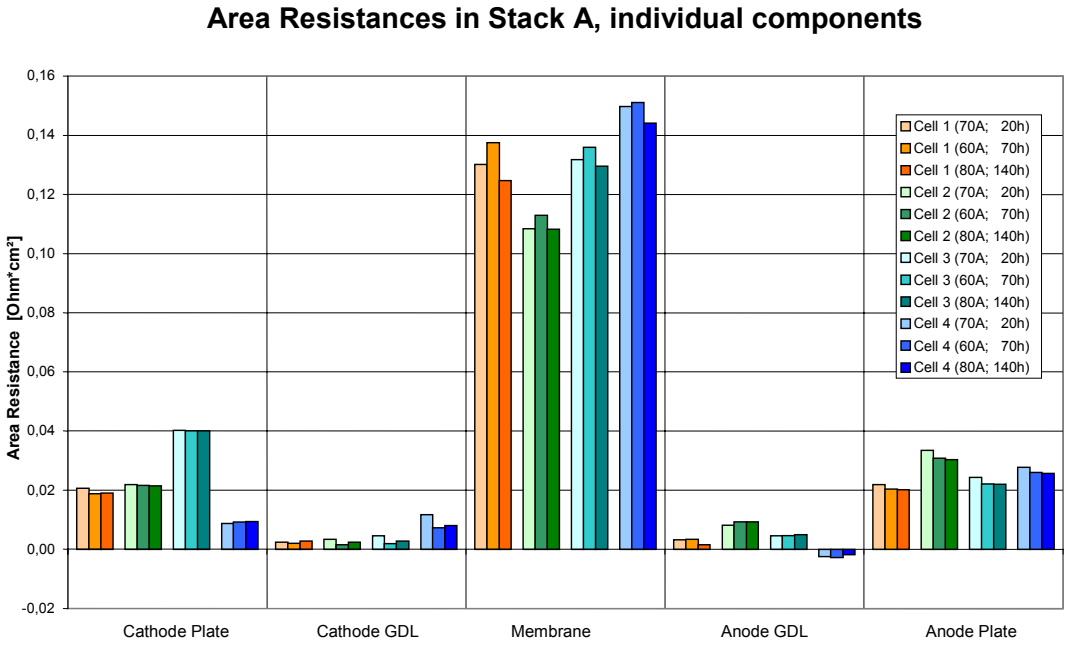

Figure 7. Area resistances of individual components of Stack **A**, calculated from impedance measurements.

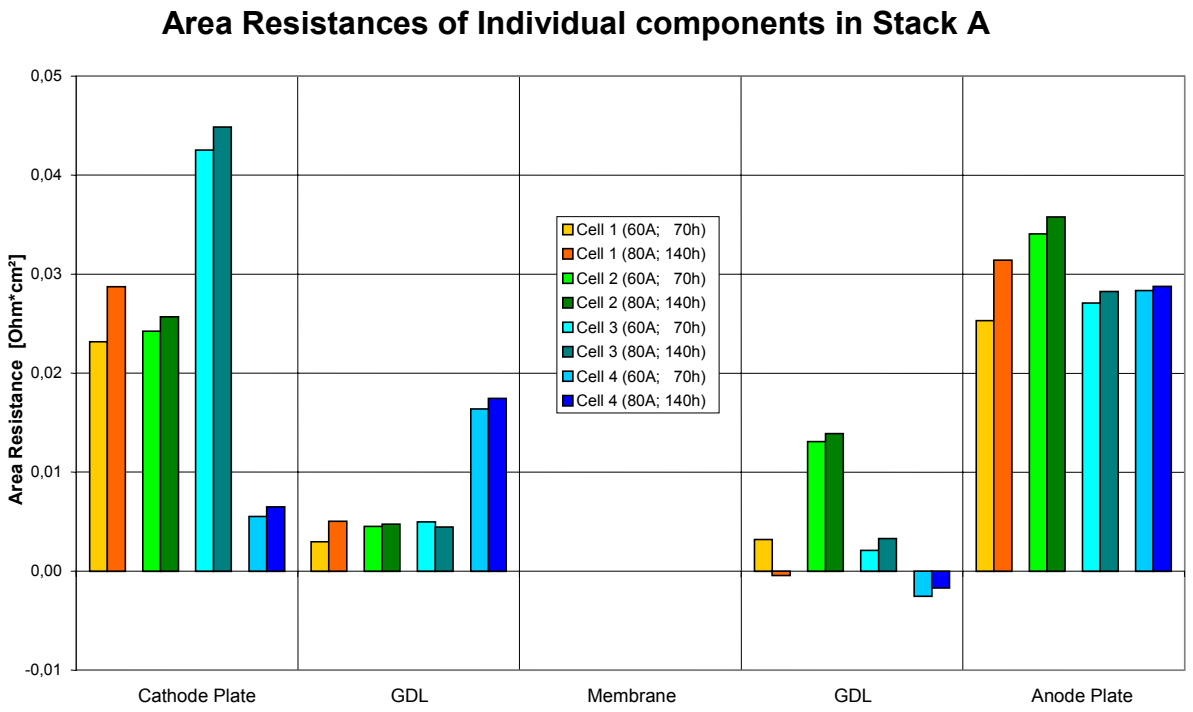

Figure 8. Area resistances of individual components with the Stack **A**, calculated from multi-meter measurements.

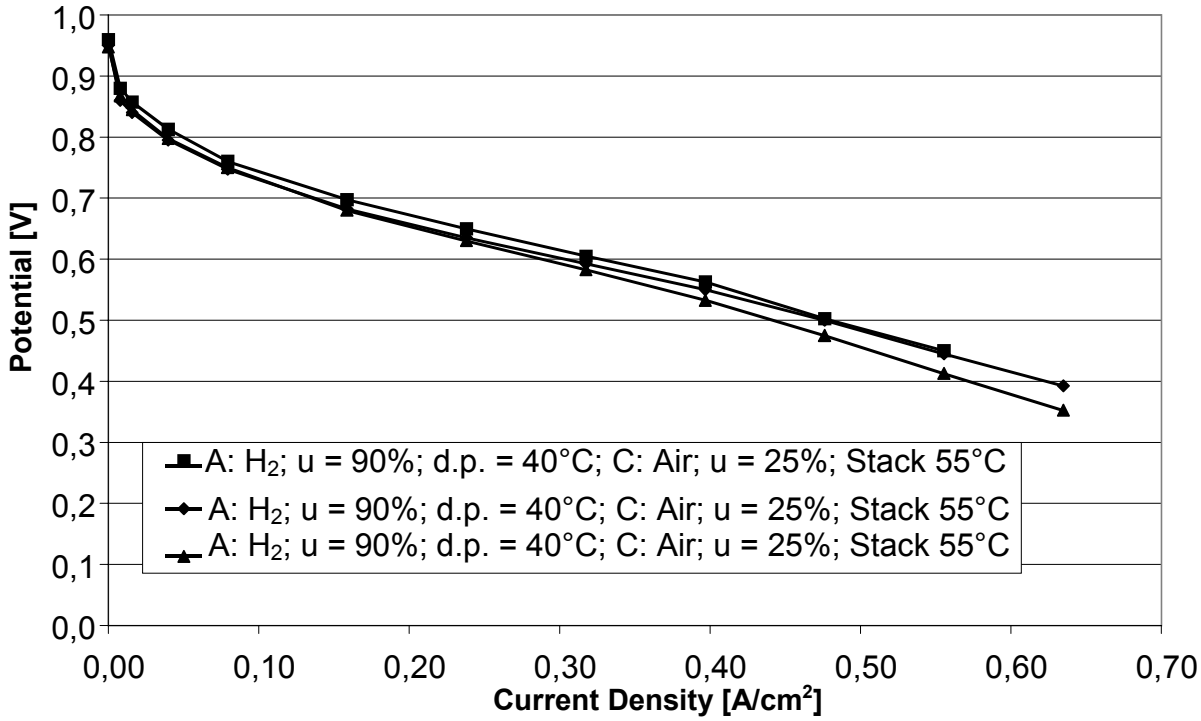

Figure 9. Polarization curves of Stack **B** at t = 0, 50, and 150 hours.

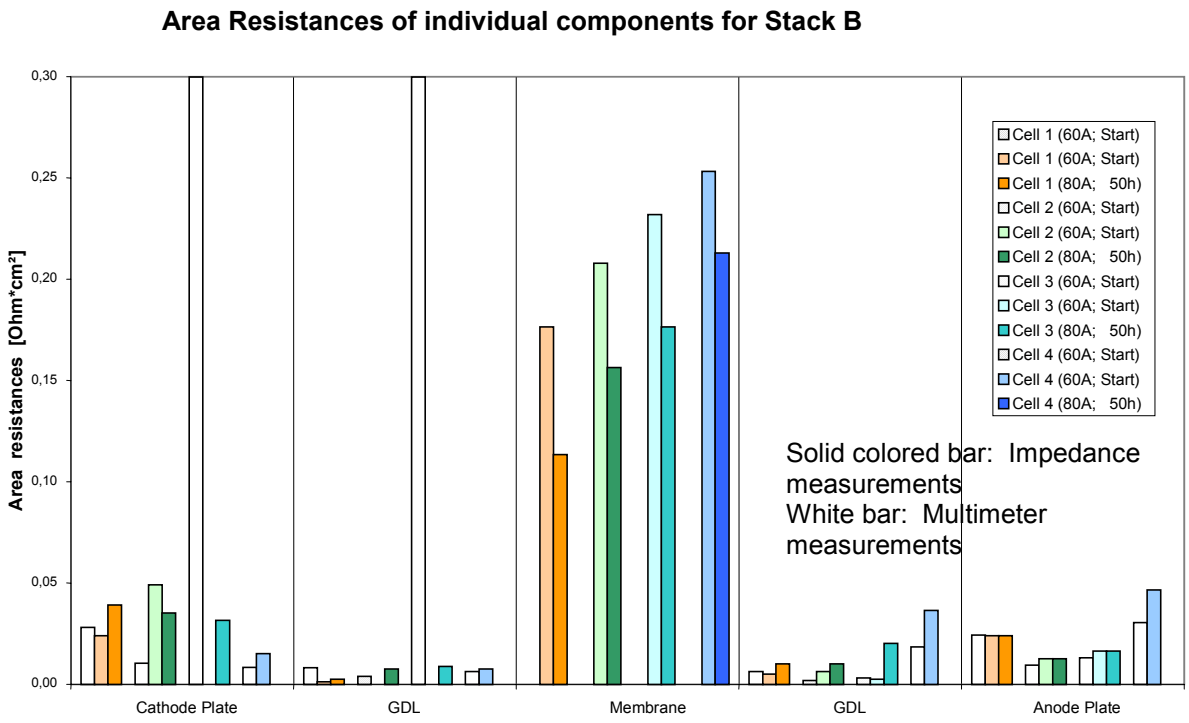

Figure 10. Area resistances of individual components from Stack **B**, calculated from multi-meter and impedance measurements.

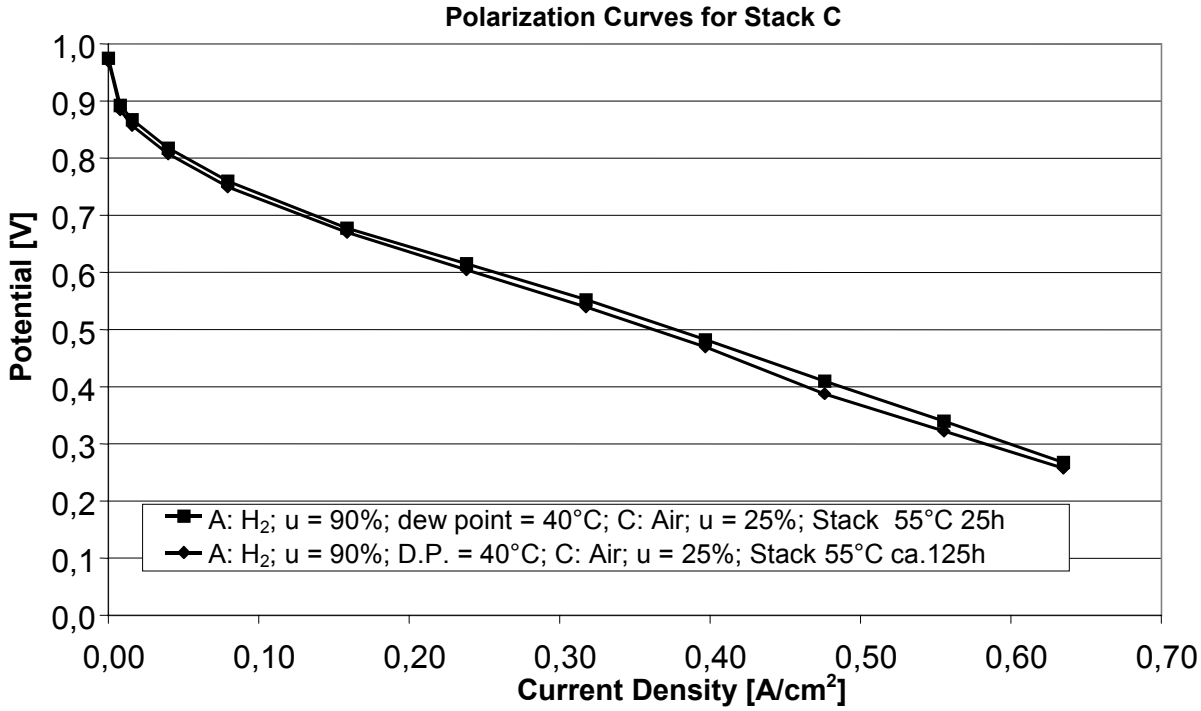

Figure 11. Polarization curves for Stack **C** at 25h and 125h.

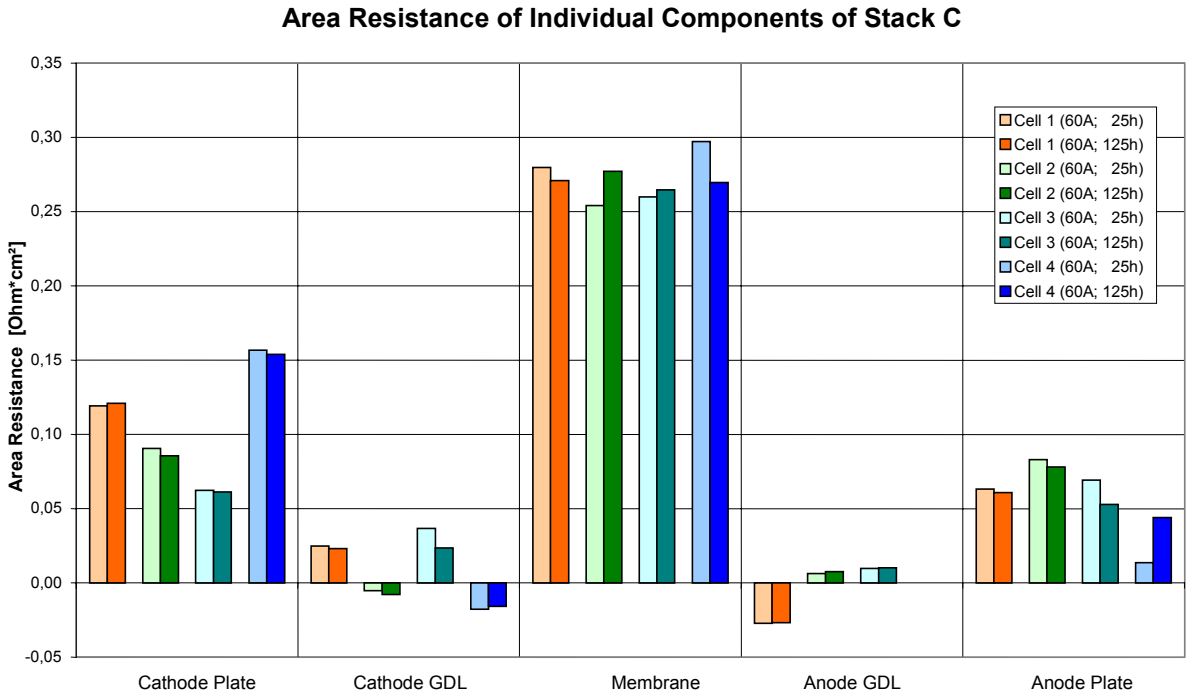

Figure 12. Area resistances of individual components of Stack **C**, calculated from impedance measurements.

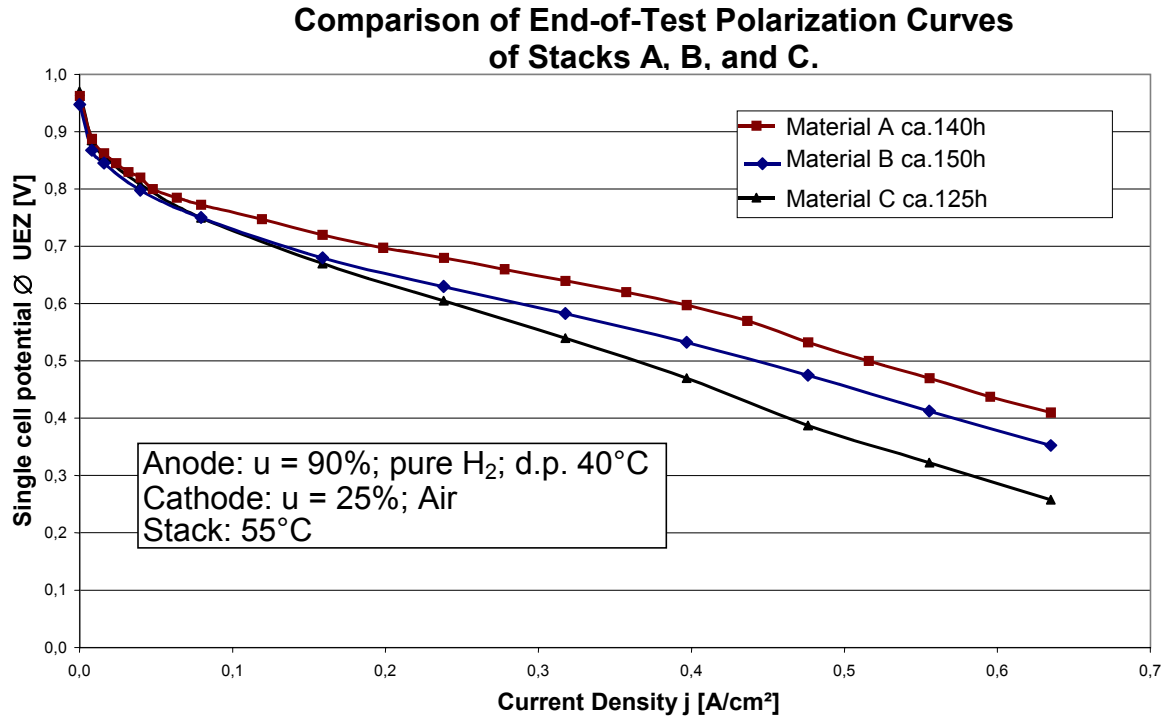

Figure 13. Comparison of the end-of-test polarization curves of Stack **A**, Stack **B**, and Stack **C**.

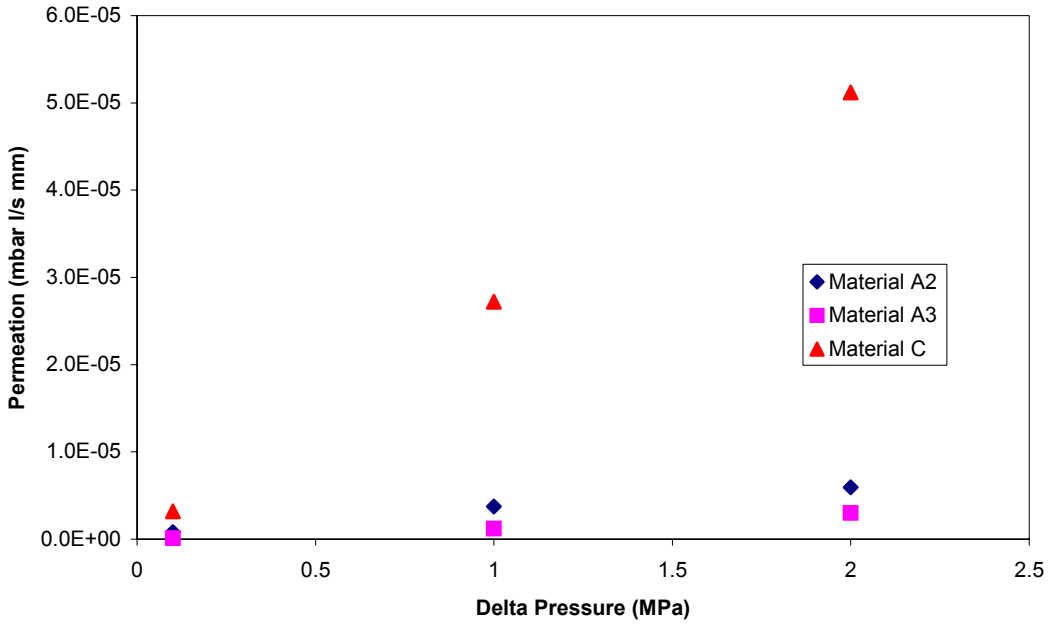

Figure 14. Helium permeation data through plate materials **A2**, **A3**, and **C**.